Adhesion of multicomponent vesicle membranes

Yanxiang Zhao*
Department of Mathematics, Pennsylvania State University, University Park, Pennsylvania 16802, USA

Sovan Das†
Department of Mechanical Engineering, Indian Institute of Technology, Kanpur 208016, India

Qiang Du‡
Department of Mathematics and Department of Materials Science and Engineering, Pennsylvania State University, University Park, Pennsylvania 16802, USA

(Received 23 December 2009; revised manuscript received 27 February 2010; published 28 April 2010)

In this work, we study the adhesion of multicomponent vesicle membrane to both flat and curved substrates, based on the conventional Helfrich bending energy for multicomponent vesicles and adhesion potentials of different forms. A phase field formulation is used to describe the different components of the vesicle. For the axisymmetric case, a number of representative equilibrium vesicle shapes are computed and a few energy diagrams are presented which reveal the dependence of the calculated shapes and solution branches on various parameters including both bending moduli and spontaneous curvatures as well as the adhesion potential constants. Our computation also confirms a recent experimental observation that the adhesion may promote phase separation in two-component vesicle membranes.

DOI: 10.1103/PhysRevE.81.041919 PACS number(s): 87.16.D−, 82.70.Uv, 68.35.Np, 87.17.Rt

I. INTRODUCTION

Adhesion is a fundamental step for many biological processes such as exocytosis, endocytosis. Cell adhesion also plays important roles in drug designs and drug deliveries as well as many biosensor applications [1,2]. There have been many experimental and theoretical studies focusing on this subject [3–7]. While many of the past studies on the vesicle-substrate adhesion have focused on the case of a flat substrate [8–14], there have also been some works that address the complexity of curved substrate. For instance, theoretical and experimental studies on the binding of a vesicle membrane to micro- or nanoparticles, or colloids have been conducted in [15–19], where the characteristic spherical substrates have radii much smaller than that of the vesicles. In [3], the adhesion of a three-dimensional vesicle to curved substrates has been studied where the curvature of the substrates is comparable to the curvature of the vesicles. A phase diagram for bound-unbound transitions has been presented. In this work, we study the adhesion of multicomponent vesicle membranes to both flat and curved substrates. This is motivated by experimental studies of the modeled subjects. For instance in a recent experiment conducted by Gordon *et al.* [4], it was observed that a mixed-lipid membrane can go through a local phase separation above critical demixing temperature due to its close proximity to a biological or non-biological surface. That is, adhesion can promote the phase separation for the mixed-lipid cell or vesicle membranes.

In this work, we develop a phase field model to study the adhesion of multicomponent vesicle membranes with a substrate through a specified adhesion potential. Following our recent approach described in [20], we take the adhesion potential to be a function of distance between the membrane and the substrate. The strength of adhesion potential is considered to be distinct for different components. By minimizing the total energy of the system that includes bending energy, interfacial line tension, and the adhesion energy, the equilibrium vesicle shapes can be computed for a variety of parameter values. As an initial attempt, we consider the case that both the vesicle membrane and the substrate are axisymmetric to simplify the computation. We present, in particular, a number of typical equilibrium two-component axisymmetric vesicle profiles undergoing adhesion. The consistency between the phase field description and its sharp interface limit is also briefly discussed. Moreover, a numerical experiment is conducted to support the conclusion of [4] that the adhesion may promote phase separation for a multicomponent membrane.

II. MULTICOMPONENT VESICLE MEMBRANE WITH ADHESION

Equilibrium shapes of a multicomponent vesicle are often described by minimizing an energy that includes elastic bending energy of the membrane and the line tension energy at the interface between the components [21]. For the elastic bending energy of vesicle membrane, a common form adopted in the literature is that introduced by Helfrich [22]

$$E_b = \int_\Gamma [\lambda(H-a)^2 + bK]d\mathbf{x}, \tag{1}$$

where Γ is the membrane surface, H and K are the mean and Gaussian curvatures of Γ with λ and b being the mean curvature bending modulus and the Gaussian curvature bending

*zhao@math.psu.edu
†sovandas@iitk.ac.in
‡qdu@math.psu.edu

modulus, respectively, and a is the spontaneous curvature. For simplicity, we consider the effect of mean curvature bending modulus and spontaneous curvature only. Thus b is set to zero and Eq. (1) becomes

$$E_b = \int_\Gamma \lambda (H-a)^2 d\mathbf{x}.$$

In this paper, we focus on two-component vesicle membranes which have the liquid-ordered and the liquid-disordered phases, and the two phases have distinct bending moduli and distinct spontaneous curvatures [23–25]. Let Γ_1 and Γ_2 be the parts of the surface representing the two different phases with λ_1, λ_2 being their corresponding bending moduli and a_1, a_2 being their corresponding spontaneous curvatures, respectively. The total elastic bending energy for the two-component vesicle is

$$E_b = \int_{\Gamma_1} \lambda_1 (H-a_1)^2 d\mathbf{x} + \int_{\Gamma_2} \lambda_2 (H-a_2)^2 d\mathbf{x}. \tag{2}$$

The line tension energy, which is essentially an interfacial energy between the two phases is given as

$$E_l = \int_{\Gamma_1 \cap \Gamma_2} \sigma dl, \tag{3}$$

where σ is the constant line tension at the interface. Equations (2) and (3) together define the total energy,

$$E = E_b + E_l, \tag{4}$$

with a minimum of E describing the shape of an equilibrium two-component closed membrane.

Note that the vesicles or membranes discussed so far are free and not bounded to other objects. To incorporate the adhesive interaction with a substrate, an additional energetic contribution due to adhesion should be added to Eq. (4)

$$E_{\text{total}} = \int_{\Gamma_1} \lambda_1 (H-a_1)^2 d\mathbf{x} + \int_{\Gamma_2} \lambda_2 (H-a_2)^2 d\mathbf{x} + \int_{\Gamma_1 \cap \Gamma_2} \sigma dl - \int_\Gamma W(\mathbf{x}) d\mathbf{x}, \tag{5}$$

where

$$W(\mathbf{x}) = \begin{cases} w_1 \cdot P(\mathbf{x}), & \mathbf{x} \in \Gamma_1 \\ w_2 \cdot P(\mathbf{x}), & \mathbf{x} \in \Gamma_2 \end{cases} \tag{6}$$

is the adhesion potential which varies with respect to the position $\mathbf{x}$ on $\Gamma = \Gamma_1 \cup \Gamma_2$. In the above, w_1 and w_2 are the corresponding strengths of the adhesion potential experienced by the liquid-ordered and the liquid-disordered phases. A representative form of W is that of a Leonard-Jones type potential form given by,

$$W(\mathbf{x}) = \begin{cases} -w_1 \cdot 4\left[\left(\frac{\beta}{d(\mathbf{x})}\right)^\alpha - \left(\frac{\beta}{d(\mathbf{x})}\right)^{\alpha/2}\right], & \mathbf{x} \in \Gamma_1 \\ -w_2 \cdot 4\left[\left(\frac{\beta}{d(\mathbf{x})}\right)^\alpha - \left(\frac{\beta}{d(\mathbf{x})}\right)^{\alpha/2}\right], & \mathbf{x} \in \Gamma_2 \end{cases} \tag{7}$$

where $d(\mathbf{x})$ is the distance from $\mathbf{x}$ to a flat/curved substrate, the constant β and the exponent α determine the thickness of the repulsive region and the rate of change in the adhesion potential, respectively. While we use the Leonard-Jones potential (7) in most of this paper, to offer a comparison, we also consider the Gaussian type potential,

$$W(\mathbf{x}) = \begin{cases} w_1 \exp(-d(\mathbf{x})^2/\epsilon^2), & \mathbf{x} \in \Gamma_1 \\ w_2 \exp(-d(\mathbf{x})^2/\epsilon^2), & \mathbf{x} \in \Gamma_2 \end{cases} \tag{8}$$

with ϵ a small number. Notice that when ϵ approaches zero, the adhesion potential converges to a sharp contact potential, a scenario that has been investigated in earlier studies [3,6].

A. Phase field formulation

To be able to effectively describe the different phases of the two-component vesicle, we use a phase field formulation which has become very popular in recent years in the modeling and simulations of vesicle deformations [20,26–31]. A phase field function can be used to describe the vesicle with the phase field bending energy as formulated in [26,27]. Adhesion energy can be incorporated into the phase field formulation as shown in [20]. For multicomponent vesicles, order parameters can be used to describe both the vesicle and its two components [32]. On the other hand, for a vesicle with a fixed topology, one can also use a direct (explicit) surface representation for the vesicle along with an order parameter (phase field function) to describe the two different phases of the membrane [30,33]. For the axisymmetric case considered here, it is particularly effective to adopt a sharp interface representation of the vesicle surface given by the revolution of a simple one-dimensional curve with an arc-length parametrization and a phase field representation of the different phases on the vesicle which is also a function of the arc length.

Specifically, let Γ be the vesicle surface, a phase field function $\eta = \eta(\mathbf{x})$ is introduced over Γ which may be used to represent either a material composition profile or a fictitious density of the lipids on the surface of the membrane and distinguishes between the liquid-ordered and liquid-disordered phases. As an illustration, we focus on the latter case so that in the liquid-ordered phase, η is specified to be $+1$ and is colored as solid blue in Fig. 1; in the liquid-disordered phase, η is assigned to be -1 and colored as dashed red. The phase field formulation described here is also commonly called diffuse interface approach or the Landau-Ginzburg formalism with $\eta = \eta(\mathbf{x})$ as the order parameter. At the interface between the liquid-ordered and liquid-disordered phases, η rapidly, but continuously, changes from $+1$ to -1. Note that the phase field regularizes the sharp interface between the two different phases into a diffused one, and thus provides a more general depiction of the two-component vesicle in both the mixed and de-mixed

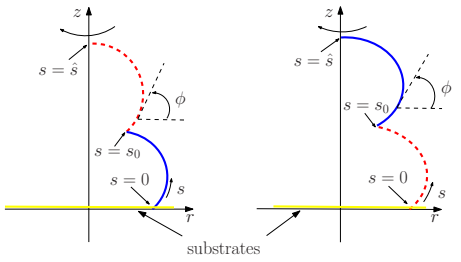

FIG. 1. (Color online) Schematic diagrams of axisymmetric two-component adhered vesicle membranes. Solid blue and dashed red colors indicate the liquid-ordered and the liquid-disordered phases, respectively. $s=s_0$ specifies the phase boundary. Away from the interface, the solid blue phase has mean curvature bending modulus c_0+c_1 and adhesion potential $w(c_0+c_2)P[d(\mathbf{x})]$, while the dashed red phase has mean curvature bending modulus c_0-c_1 and adhesion potential $w(c_0-c_2)P[d(\mathbf{x})]$.

states. The total energy (5) of the model in terms of the phase function η is given by

$$E(\eta) = \int_\Gamma (c_0 + c_1\eta)[H - a(c_0 + c_3\eta)]^2 d\mathbf{x} + \sigma \int_\Gamma \left[\frac{\xi}{2} |\nabla_\Gamma \eta|^2 + \Phi(\eta) \right] d\mathbf{x} - \int_\Gamma w(c_0 + c_2\eta) P[d(\mathbf{x})] d\mathbf{x}, \tag{9}$$

where the first and third terms are phase field formulas for elastic bending energy and adhesion energy, respectively. The term $c_0+c_1\eta$ is a phase field representation of λ_1 and λ_2. When $\mathbf{x}$ is away from the interfacial region, $c_0+c_1=\lambda_1$ and $c_0-c_1=\lambda_2$. The liquid-ordered phase is stiffer than the liquid-disordered phase, hence we always assume $c_1>0$. The term $a(c_0+c_3\eta)$ is considered as the phase field analog of spontaneous curvature, and

$$a(c_0 + c_3) = a_1, \quad a(c_0 - c_3) = a_2$$

if $\mathbf{x}$ is away from the interfacial region. Similarly, $w(c_0+c_2\eta)P[d(\mathbf{x})]$ is viewed as an approximation of the adhesion potential $W(\mathbf{x})$, with

$$w(c_0 + c_2) = w_1, \quad w(c_0 - c_2) = w_2$$

when $\mathbf{x}$ is far away from the interfacial region. The second term is a phase field approximation for the line tension energy where a double well potential function

$$\Phi(\eta) = \frac{1}{4\xi}(\eta^2 - 1)^2 \tag{10}$$

is incorporated. $\nabla_\Gamma \eta$ is the surface gradient of η, which is the projection of $\nabla\eta$ onto the tangent plane of Γ. Notice that to make $\nabla_\Gamma \eta$ well defined, the function η should be defined away from the membrane such that $d\eta/d\mathbf{n}=0$ where $\mathbf{n}$ is the normal vector of Γ. The enclosed volume and total area of the membrane are assumed to be invariant. Meanwhile, the total amount of lipids is conserved. Thus, three constraints are imposed during the minimization of the total energy (9):

$$\int_\Gamma d\mathbf{x} = A, \quad \int_\Gamma dV = \mathrm{Vol}, \quad \int_\Gamma \eta(\mathbf{x}) d\mathbf{x} = C. \tag{11}$$

The constraint $\int_\Gamma \eta(\mathbf{x})d\mathbf{x}=C$ denotes the difference in the surface areas of the two phases in the sharp interface limit.

B. Axisymmetric setting

In the present work, we focus on the axisymmetric membrane adhered on a flat/curved substrate. In this setting, the membrane surface is determined by revolving a two-dimensional curve. A vesicle with a flat substrate is schematically shown in Fig. 1. The curve is parameterized by the arc-length s, and the total length of the curve is denoted by $\hat{s}$. The flat substrate is located at $z=0$ with the two different phases being distinguished by the dashed red and solid blue colors. The transition point from dashed red to solid blue is located at $s=s_0$. The figures on the left and right show different configurations with the solid blue phase and the dashed red phase being adjacent to the substrate, respectively. For easy reference, we denote the left as *red-blue* vesicle membrane, and the right as *blue-red* vesicle membrane. The tangent angle ϕ is measured from the radial direction and r is the distance of a point on the membrane from the axis of symmetry.

The mean curvature of the vesicle can be explicitly expressed by r and ϕ as

$$H = \frac{1}{2}\left(\phi' + \frac{\sin\phi}{r} \right),$$

where prime represents the derivative with respect to arc-length s. The line tension energy term in Eq. (9) becomes

$$2\pi\sigma \int_0^{\hat{s}} \left[\frac{\xi}{2}\eta'^2 + \frac{1}{4\xi}(\eta^2 - 1)^2 \right] r ds.$$

We nondimensionalize all the parameters and choose c_0 to be 1. Then the phase field model (9) is reduced to

$$E(\eta) = 2\pi \int_0^{\hat{s}} (1 + c_1\eta)[H - a(1 + c_3\eta)]^2 r ds + 2\pi\sigma \times \int_0^{\hat{s}} \left[\frac{\xi}{2}\eta'^2 + \frac{1}{4\xi}(\eta^2 - 1)^2 \right] r ds - 2\pi \int_0^{\hat{s}} w(1 + c_2\eta) P[d(\mathbf{x})] r ds. \tag{12}$$

Additionally, the constraints (11) in the axisymmetric case lead to

$$(\cos T)' = -r, \tag{13}$$

with T being the arc-length parameter of the reference unit sphere,

$$\pi \int_0^{\hat{s}} r^2 z' ds = \mathrm{Vol}, \tag{14}$$

and

$$\int_0^{\hat{s}} \eta(s) r ds = C. \tag{15}$$

The pointwise constraint (13), which is in fact equivalent to the one in Eq. (11), is referred as the lateral incompressibility condition for the membrane [34].

The shape of the membrane is determined by minimizing the total energy (12), subject to constraints (13)–(15). It satisfies the Euler-Lagrange equations given by

$$\left[\tilde{H}'' + \frac{r'\tilde{H}'}{r} + 2\tilde{H}(H^2 - K) + 2a\tilde{H}H(1 + c_3\eta)\right] - 2(\mu H + p + \tau\eta H) + \sigma\xi\eta'^2\phi' - \sigma H[\xi\eta'^2 + 2\Phi(\eta)] - w(1 + c_2\eta)\left\{\frac{\delta P}{\delta n} - 2HP\right\} = 0, \tag{16}$$

$$c_1[H - a(1 + c_3\eta)]^2 - 2ac_3\tilde{H} + \tau - c_2 wP + \sigma \times\left[-\xi\left(\eta'' + \frac{r'\eta'}{r}\right) + \frac{d\Phi}{d\eta}\right] = 0, \tag{17}$$

where $\tilde{H} = (1 + c_1\eta)[H - a(1 + c_3\eta)]$ and μ, p and τ are the three Lagrange multipliers for the three constraints, respectively. The other equations from geometry are [25,35]

$$\phi' = 2H - \frac{\sin\phi}{r}, \quad r' = \cos\phi, \quad z' = \sin\phi. \tag{18}$$

Boundary conditions are imposed as follows:

$$H'(0) = H'(\hat{s}) = 0; \quad r(0) = r(\hat{s}) = 0;$$

$$\phi(0) = 0, \quad \phi(\hat{s}) = \pi; \quad \eta'(0) = \eta'(\hat{s}) = 0. \tag{19}$$

III. NUMERICAL EXPERIMENTS

We numerically solve Eqs. (16)–(18) subject to boundary condition (19) using the MATLAB ODE solver BVP4C. We tested the convergence of the computed results in our numerical simulation.

A. Adhesion with Leonard-Jones potential

We first present the numerical results of a few adhered vesicles using the Leonard-Jones adhesion potential.

In the axisymmetric setting, two typical vesicle shapes, adhered *prolate* and adhered *oblate*, are presented. Note that for single component vesicle membrane, one of these two shapes is always energetically favorable than the other when adhesion strength $w > w_a(v)$ with $w_a(v)$ representing the critical adhesion strength, and the reduced volume $v \geq v_2$ with v_2 representing the transition volume from adhered stomatocyte to adhered oblate [36]. However, for two-component vesicles, the energetics of adhered prolate and adhered oblate shapes depend on the competition between the line tension σ and adhesion strength w for a fixed volume. A phase diagram, for transition between adhered prolate and adhered oblate shapes in $\sigma - w$ parameter space, is shown in Fig. 2.

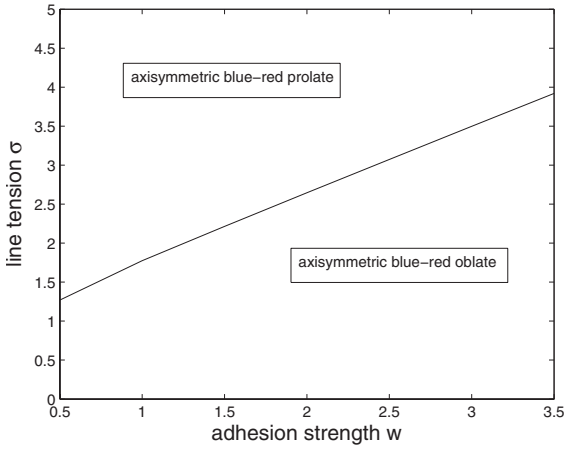

FIG. 2. Phase transition from prolate vesicle to oblate vesicle in the axisymmetric case. Area$=4\pi$, volume$=3.0$, area difference $C=-0.3$, $c_1=0.4$, $c_2=-0.5$ $c_3=0$, $a=0$, $\xi=0.01$, $\alpha=5$, $\beta=0.05$.

The other parameters, area$=4\pi$, volume$=3.0$, $C=-0.3$, $c_1=0.4$, $c_2=-0.5$, $c_3=0$, $a=0$, $\xi=0.01$, $\alpha=5$, and $\beta=0.05$ are fixed. The reason we take blue-red adhered vesicles as representative shapes in each stability region is because the axisymmetric blue-red adhered vesicle always has lower energy than the red-blue adhered vesicle for negative values of c_2, which will be shown later on in this subsection. Near $w=0.5$, the two-component axisymmetric adhered oblate vesicle transits into an *almost* free vesicle. By *almost* we mean the vesicle is adhered to the substrate only at the two tips of a cross sectional view (note that the free oblate is convex in the blue part and concave in the red part with the given parameters). Referring to the discussion in [37], we believe that when the axisymmetric adhered oblate is energetically favorable than the axisymmetric adhered prolate, it is more likely a globally minimizer (at least it is in the axisymmetric setting). When the axisymmetric adhered prolate is favorable, it might be only a local minimizer as the nonaxisymmetric prolate might have lower energy than the axisymmetric prolate. However, the nonaxisymmetric prolate is beyond the scope of our modeling, and we focus on the axisymmetric adhered oblate shape. We also briefly discuss the axisymmetric adhered prolate shapes.

In Fig. 3, several numerical solutions for Eqs. (16)–(19) are shown. The curves are the cross sections of the adhered oblates with the solid blue region representing the liquid-ordered phase and the dashed red region representing the liquid-disordered phase. The corresponding parameter values used in the experiments are taken as area$=4\pi$, volume$=3.5$, $C=-0.3$, $\sigma=2$, $c_1=0.4$, $c_3=0$, $a=0$, $\xi=0.01$, $\alpha=5$, $\beta=0.05$. Note that $c_1=0.4$ implies that the ratio $\lambda_{\text{blue}}/\lambda_{\text{red}}$ of the mean curvature bending moduli between the blue and red phases is 1.4/0.6. Moreover, $a=0$ and $c_3=0$ imply that both phases have zero spontaneous curvature. Blue-red adhered oblate vesicles on flat substrate are shown in Fig. 3(a) where $c_2=-0.5$, that is, $w_{\text{blue}}/w_{\text{red}}=1/3$. Except the adhesion strength w, all the parameters are kept fixed as specified. Some adhered shapes of red-blue oblate vesicles are shown in Fig. 3(b) for various w and $c_2=0.5$.

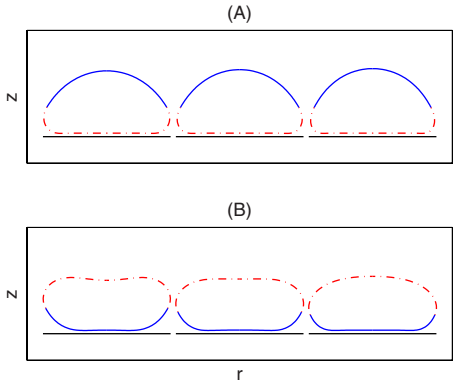

FIG. 3. (Color online) Adhered oblate membrane shapes for different w. Area$=4\pi$, volume$=3.5$, area difference $C=-0.3$, $\sigma=2$, $c_1=0.4$, $c_3=0$, $a=0$, $\xi=0.01$, $\alpha=5$, $\beta=0.05$; (a) $c_2=-0.5$, $w=2.0, 4.0, 8.0$, from left to right; (b) $c_2=0.5$, $w=2.0, 4.0, 8.0$, from left to right.

Figure 4 shows the energy comparison between blue-red oblate membrane and red-blue one under the influence of adhesion. Here, area$=4\pi$, volume$=3.5$, $C=-0.3$, $\sigma=2$, $c_1=0.4$, $c_3=0$, $a=0$, $\xi=0.01$, $\alpha=5$, $\beta=0.05$, $w=2.0$ are fixed. The two shapes on the left correspond to parameter $c_2=-0.2$ with $w_{\text{blue}}/w_{\text{red}}=0.8/1.2$. The blue-red oblate, which is more deformed from the free oblate shape, has lower energy and is more energetically favorable than the red-blue one in this case. On the other hand, the two shapes on the right correspond to $c_2=0.5$ leading to $w_{\text{blue}}/w_{\text{red}}=1.5/0.5$. There, the red-blue oblate is more favorable than the blue-red one.

The energy comparison of the four shapes as discussed above may lead us to believe that the vesicle whose component adjacent to the substrate endures stronger adhesion is more stable. However, this is not always the case. As seen in Fig. 4, there is an anomalous region with c_2 between zero and 0.2438, and the blue phases suffer stronger adhesion but the blue-red oblate is more stable. Outside this region, the shape with stronger adhesion on the component adjacent to the substrate is more stable. We observe that the existence of the region (0, 0.2438) is due to the nonzero values of c_1 and C which model, in the two-component system, the effects due to the differences in the bending moduli and the surface areas of the two phases. When both c_1 and C approach zero, which is the limit where both components have the same bending moduli and equal surface areas, the multicomponent vesicle reduces into a single component vesicle. And the anomalous region shrinks to the point $c_2=0$, also the transition point converges to $c_2=0$.

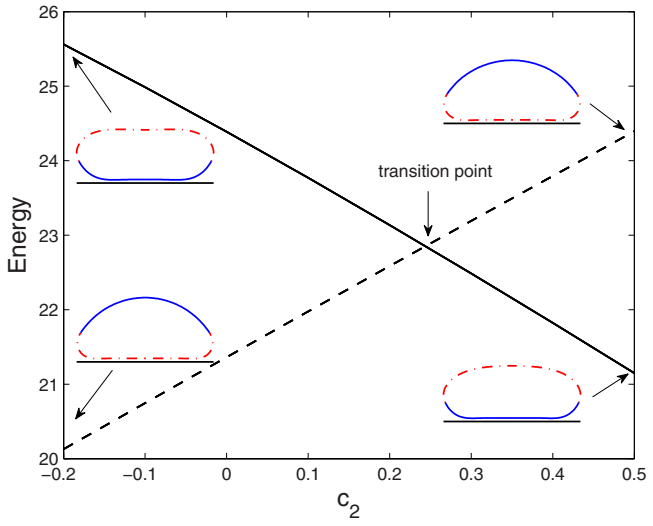

FIG. 4. (Color online) Energy comparison between blue-red adhered oblate and red-blue adhered one. $w=2$, $c_1=0.4$ are fixed. c_2 varies from −0.2 to 0.5. The solid curve represents energy versus c_2 for the red-blue oblate, while the dash curve is for the blue-red oblate. The shapes of the vesicles at the four end-points of the curves are shown. Area$=4\pi$, volume$=3.5$, area difference $C=-0.3$, $\sigma=2$, $c_3=0$, $a=0$, $\xi=0.01$, $\alpha=5$, $\beta=0.05$.

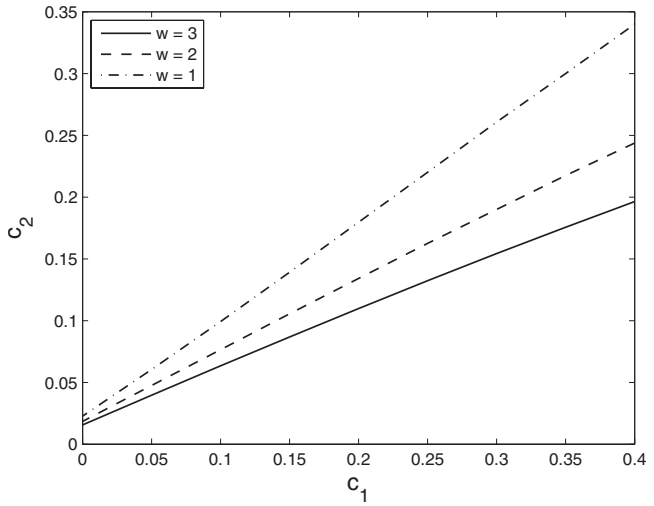

FIG. 5. Transition curves of blue-red/red-blue adhered oblate for $w=1.0, 2.0, 3.0$. Above each curve, red-blue oblate is more stable; the blue-red oblate is more stable below the curves. The other parameter values are: Area$=4\pi$, volume$=3.5$, area difference $C=-0.3$, $\sigma=2$, $c_3=0$, $a=0$, $\xi=0.01$, $\alpha=5$, $\beta=0.05$.

In addition, the transition point in Fig. 4 strongly depends on c_1 and the adhesion potential w. The dependence of the transition points on c_1 is shown in Fig. 5. For various $w=3.0$, 2.0, and 1.0, we plot the transition curve c_1 versus c_2. The red-blue adhered oblate, corresponding to the parameter pair (c_1, c_2) above each curve, is more favorable; while the blue-red adhered oblate is more favorable if the parameters c_1, c_2 are chosen from the region below the transition curves.

Figure 5 shows that the transition always occurs for $c_2>0$. One may wonder if this is universally true for any adhesion potential w. The answer is provided via Fig. 6, the transition curve w vs c_2 for fixed $c_1=0.4$. In Fig. 6, the solid curve corresponds to the blue-red/red-blue transition for the adhered oblate vesicle, while the dashed curve corresponds to blue-red/red-blue transition for the adhered prolate vesicle. For the oblate vesicle, w varies from 0.59 to 6.5; while for the prolate vesicle, w varies from 0.00 to 6.5. Above each transition curve, the red-blue vesicle is the energetically more favorable one; while below the curve, the blue-red vesicle is more favorable. The prolate vesicle continuously changes from a bound state to a free state as w decreases from 6.5 to 0. As w becomes sufficiently small, the

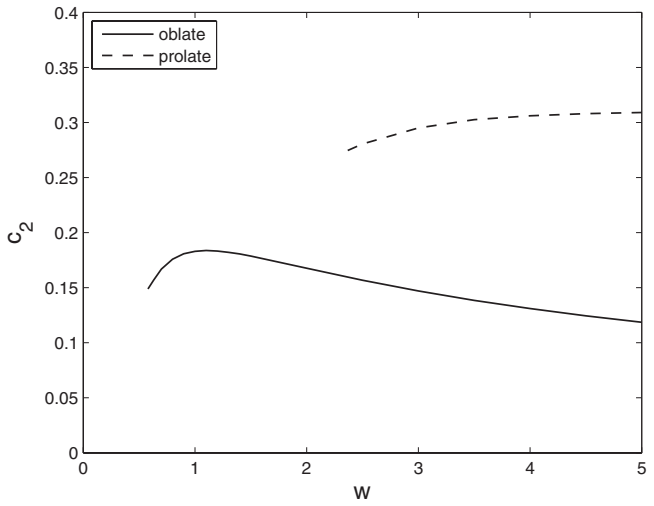

FIG. 6. Dependence of c_2 on w for phase transition when $c_1=0.4$. Area$=4\pi$, volume$=3.5$, area difference $C=-0.3$, $\sigma=2$, $c_3=0$, $a=0$, $\xi=0.01$, $\alpha=5$, $\beta=0.05$.

prolate vesicle is only adhered via the south pole, but still energetically lower than the free prolate vesicle. The oblate vesicle behaves in a different way. As w decreased from 6.5 to 0.59, the lower part of the oblate vesicle are entirely adhered to the substrate. Near $w=0.59$, the blue-red oblate vesicle transits into an almost free state which is similar to the phenomenon in Fig. 2. One may wonder if c_2 becomes negative for large enough values of w. If we assume that c_2 becomes negative for some large enough w, then adhesion energy of the blue-red oblate is much greater than that of red-blue oblate. Consequently, adhesion energy becomes dominant over bending and line tension energies, and it is unlikely that a transition between blue-red and red-blue vesicles occurs for such values of (w,c_2). Actually, as w becomes larger and larger, we numerically reveal that c_2 asymptotically goes to 0.31 and 0.00 for prolate and oblate vesicles, respectively.

We have, so far, considered the phase transition of oblate vesicles. It is also of interest to study the prolate vesicles and related stability issues. Due to the similarities in the numerical experiments, we do not repeat the phase diagram of c_1,c_2 and w for the prolate case. Instead, we consider the effects of the spontaneous curvature and the substrate curvature [38,39] and discuss the stability of prolate vesicle under the influence of these parameters.

In Fig. 7, the flat substrate is now replaced by a concave-up spherical substrate with radius $R=3$. Here, area $=4\pi$, volume$=2.7$, area difference $C=0$, $\sigma=1$, $c_1=0$, $c_2=0$, $c_3=0.5$, $a=2/3$, $\xi=0.01$, $\alpha=5$, and $\beta=0.05$. We take $w=0$ and $w=2$, respectively, to find both free prolate vesicles and adhered prolate vesicles. Differing from the previous figures in this subsection, the red and blue colors in this experiment indicate the phases having different spontaneous curvatures. The blue phase has a bigger spontaneous curvature $a(1+c_3)=1$ while the red phase has a smaller one $a(1-c_3)=1/3$. A1 and B1 show the free prolate with specified parameters. Notice that the red phase, which possesses a smaller spontaneous curvature, has shapes less elongated than the blue phase. A2 and B2 are adhered blue-red and

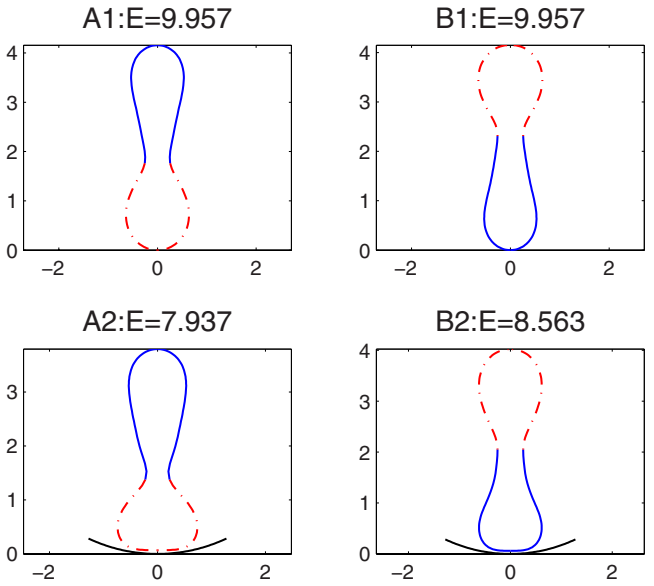

FIG. 7. (Color online) Effect of spontaneous curvatures on the prolate vesicles. Representative shapes of prolate vesicles are shown. Area$=4\pi$, volume$=2.7$, area difference $C=0$, $\sigma=1$, $c_1=0.0$, $c_2=0$, $c_3=0.5$, $a=2/3$, $\xi=0.01$, $w=2$, $\alpha=5$, $\beta=0.05$.

red-blue prolate vesicles. By comparing their total energy, we find out that the blue-red prolate vesicle with the red phase at bottom, whose spontaneous curvature matches with the curvature of the curved substrate, is more stable than the red-blue prolate vesicle.

We choose here a volume of 2.7, which is smaller than the previously chosen value of 3.5 because larger osmotic pressure difference makes the effect of spontaneous curvatures on the vesicle shapes more visible.

Similar to the discussion of stability transition in Figs. 5 and 6, when the spontaneous curvature effect is taken into account, we can also find the dependence of transition points on c_1,c_2,c_3,w. Without repeatedly showing many figures, we present here only the transition curve c_3 vs c_2 in Fig. 8 with $c_1=0,w=2$ fixed. Other parameters are set as area $=4\pi$, volume$=2.7$, area difference $C=0$, $\sigma=1$, $a=2/3$, $\xi=0.01$, $\alpha=5$, and $\beta=0.05$. Above the transition curve, the red-blue prolate vesicle is more energetically favorable than the blue-red prolate vesicle; while below the transition curve, the blue-red prolate vesicle is more favorable.

B. Adhesion with Gaussian potential

Another possible adhesion potential can be applied in our model is the Gaussian adhesion potential (8).

Few axisymmetric numerical solutions of prolate vesicles are presented in Fig. 9. Notice that there is a slight protrusion of prolate vesicles into the flat substrate. This is due to the lack of repulsive effect in the Gaussian form of the adhesion potential.

Convergence of the adhered prolate vesicle as ϵ approaches zero is presented in Fig. 10. Theoretically, by the standard asymptotic analysis, η tends to converge to $\tanh(\frac{s-s_0}{\sqrt{2}\xi})$ when ξ approaches zero, where s_0 indicates the

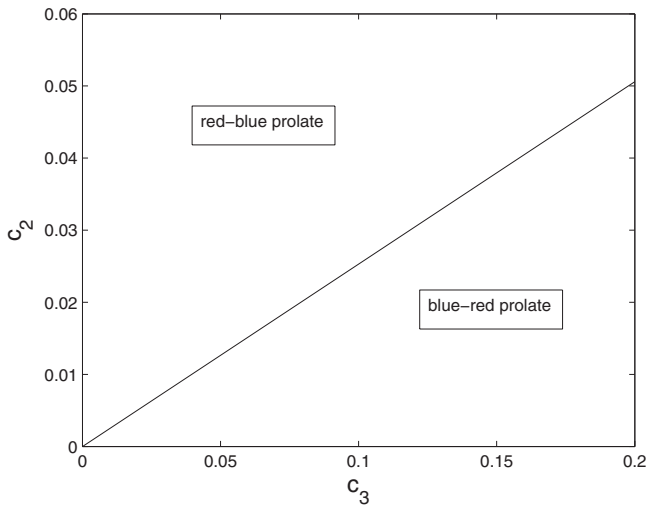

FIG. 8. Dependence of c_2 on c_3 for phase transition. Red-blue prolate is more energetically favorable for (c_3,c_2) from above the transition curve; while the blue-red prolate is more favorable for (c_3,c_2) from below the transition curve. area$=4\pi$, volume$=2.7$, area difference $C=0$, $\sigma=1$, $c_1=0.0$, $a=2/3$, $\xi=0.01$, $\alpha=5$, $\beta=0.05$, $w=2$.

location of the interface which depends on the area difference C (see Appendix). Numerically, for relatively larger ϵ, the shapes of two-component vesicle membranes protrude into the flat substrate more significantly. As ϵ gets smaller, the protrusion becomes less visible and finally vanishes in the limit of $\epsilon \to 0$, that is the case corresponding to the effective contact potential [3,6,20]

$$W(\mathbf{x}) = \begin{cases} w & d(\mathbf{x}) = 0 \\ 0 & \text{otherwise}. \end{cases} \tag{20}$$

The stability transition curves, similar to that obtained previously for Leonard-Jones type potential, can also be obtained for Gaussian potential. Given the similarities in the findings, we do not repeat the discussion here.

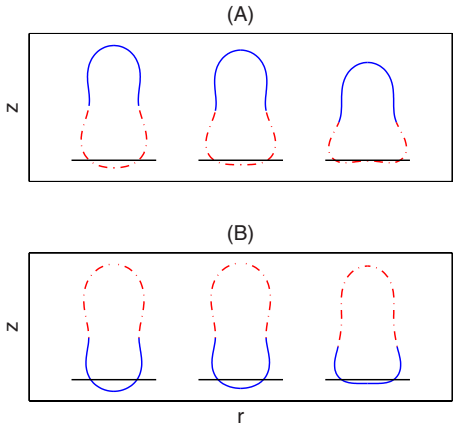

FIG. 9. (Color online) Adhered prolate membrane shapes for different w with Gaussian adhesion potential. Area$=4\pi$, volume $=3.5$, area difference $C=-0.3$, $\sigma=2$, $c_1=0.4$, $c_3=0$, $a=0$, $\xi=0.01$, $\epsilon=0.15$; (a) $c_2=-0.05$, $w=1.0,1.5,2.0$, from left to right; (b) $c_2=0.2$, $w=2.0,3.0,5.0$, from left to right.

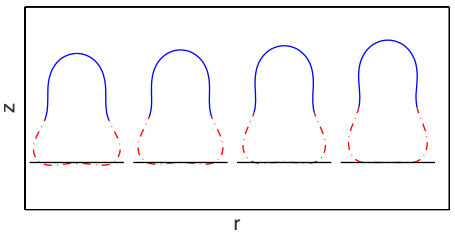

FIG. 10. (Color online) Convergence of adhered prolate membranes as $\epsilon \to 0$. $\epsilon=0.15,0.10,0.05,0.01$, from left to right. Area $=4\pi$, volume$=3.5$, area difference $C=-0.3$, $\sigma=2$, $c_1=0.4$, $c_2=-0.05$, $c_3=0$, $a=0$, $\xi=0.01$, $w=2$.

C. Promotion of phase separation

In this section, three numerical experiments are presented to support Gordon and co-workers' experimental observation that adhesion may promote the phase separation [4]. Similar discussion can be found in [40–43] where the authors consider planar membranes that are entirely attached to corrugated substrates.

The experiments involve the phase field simulations for relatively large diffuse interface width parameter ξ which is consistent to the experimental setting. The Leonard-Jones type adhesion potential is employed in this subsection.

In the first experiment, the function $\eta(s)$ is viewed as a chemical composition function, which can be considered as a compositional fluctuation around a homogeneous state with composition η_0. The constraint (15) is specified as

$$\int_0^{\hat{s}} \eta(s) r ds = \int_0^{\hat{s}} \eta_0 r ds. \tag{21}$$

We now demonstrate that for an equilibrium free oblate vesicle with associated $\eta(s)$ almost homogeneous, namely, $\eta(s) \approx \eta_0$, after adding the adhesion, it displays the phase separation behavior with $\eta(s)$ changing into a tanhlike profile representing two distinct phases.

The numerical experiment is presented in Fig. 11. In plots A1 and A2, for area$=4\pi$, volume$=3.5$, $\eta_0=-1/\sqrt{3}$, $\xi=0.33$, $\sigma=5/(1-0.8\eta_0)$, $c_1=0.8/(1-0.8\eta_0)$, $c_2=1.0/(1-1.0\eta_0)$, $c_3=0$, $a=0$, a free oblate vesicle is computed first. The chemical composition function η and the associated vesicle profile shown in plots A1 and A2 correspond to the stable energy minimum (in the absence of adhesion). The change in composition is relatively small, representing a state of mixed phases in much of the vesicle. By adding Leonard-Jones adhesion with $w=5(1-1.0\eta_0)/(1-0.8\eta_0)$, $\beta=0.023$, $\alpha=5$, an adhered vesicle with associated η corresponding to the new energy minimizer is shown in plots B1 and B2. A phase separation occurs with a much more significant phase difference $\max(\eta)-\min(\eta)=1.9703$ in plot B2. In comparison, we have $\max(\eta)-\min(\eta)=0.2345$ in plot A2, which is only 11.90% of the phase difference for adhered vesicle. We thus see that adhesion can significantly promote phase separation. Furthermore, the bending modulus of the phase-mixed vesicle λ_{mixed} is roughly around $1/(1-0.8\eta_0)$, and the bending moduli of the phase-separated vesicle are $\lambda_{\text{blue}}=2.2649/(1-0.8\eta_0)$ and $\lambda_{\text{red}}=0.6873/(1-0.8\eta_0)$. These parameter values imply that $\lambda_{\text{red}} \approx \lambda_{\text{mixed}}$ and $\lambda_{\text{blue}}/\lambda_{\text{red}}$

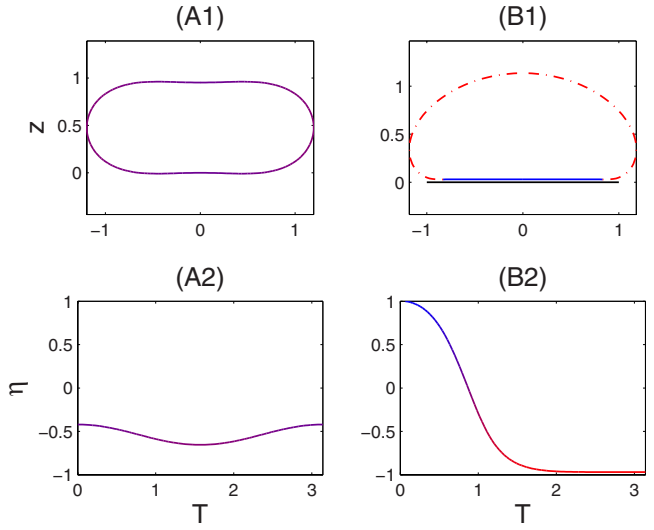

FIG. 11. (Color online) Adhesion induces phase separation. An almost homogeneous free oblate vesicle is phase-separated by a Leonard-Jones adhesion.

=3.2954, which agree with the ratios of the bending stiffnesses of the ordered, the disordered and the mixed phases available in the literature [4,23,24,44].

Another numerical experiment is presented in Fig. 12 where a stairlike substrate is considered. In plots A1 and A2, for area=4π, volume=3.515, η_0=0.5, ξ=0.22, σ=0.1/(1 −0.112η_0), c_1=0.112/(1−0.112η_0), c_2=0.007/(1−0.007 η_0), c_3=0, a=0, we plot the computed shape of the free oblate vesicle together with the changes in the associated mean curvature H along the cross section. Then in plots B1 and B2, we show the computed adhered oblate vesicle with stairlike substrate where w=110(1−0.112η_0)/(1−0.007η_0), β=0.047, α=5, and the associated mean curvature H. In this example, both curvature and adhesion play important roles in the phase separation. The liquid-ordered phase is observed in

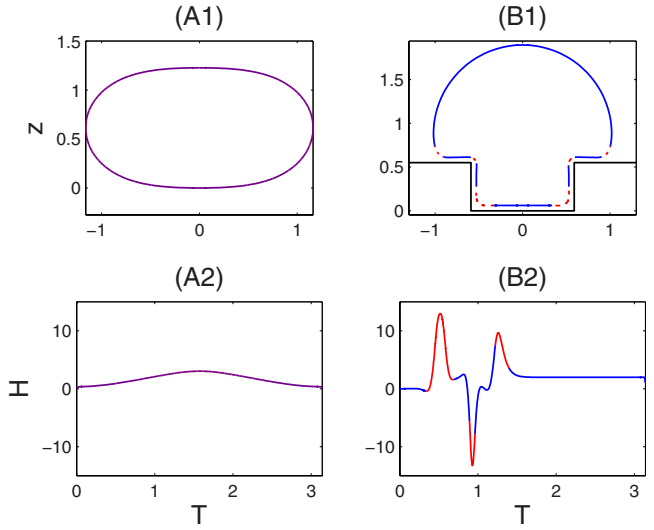

FIG. 12. (Color online) Adhesion induced phase separation with stairlike substrate. An almost homogeneous free oblate vesicle is phase-separated by a Leonard-Jones adhesion. The red phase (dashed) is observed in the region with high curvature.

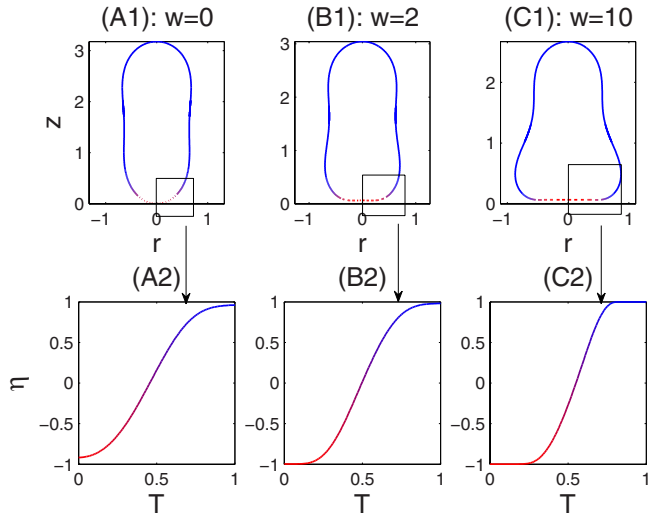

FIG. 13. (Color online) Promotion of phase separation. As w gets bigger, the two phases of η near the interfacial region are separated more. Area=4π, volume=3.5, area difference C=1.7, ξ =0.13, σ=1, c_1=0.05, c_2=−1.00, c_3=0, ζ=1, β=0.05, α=5.

the regions where the membrane is either attached to the flat part of the substrate or in the detached part with lower curvature while the liquid-disordered phase localizes in the regions with high curvature. Similar curvature dependent phase separation in the context of the adhesion of translationally symmetric membranes and substrates has been observed in [42].

The effect of adhesion on phase separation can be further demonstrated in the next experiment. Here again, we take the order parameter $\eta(s)$ to be a labeling function for relative lipid density which stays within $[-1,1]$. To model a wider diffuse interfacial layer corresponding to a relatively large ξ and yet maintain the bound on η, we replace the double well potential function (10) by the following double obstacle potential function [45]:

$$(1+\eta)\ln(1+\eta)+(1-\eta)\ln(1-\eta)+\gamma(1-\eta^2)-2\ln 2. \tag{22}$$

where γ=1+2 ln 2 is a constant describing the height of the potential barrier.

Figure 13 shows a numerical experiment while we choose ξ=0.13 so that for unbounded prolate vesicles, there would be a wide interfacial regions with less dramatic phase separation effect. Then for various w=0, 2, and 10, we compute the corresponding adhered prolate vesicles and the corresponding lipid density functions η. We highlight the densities near the interfacial region (the boxed portion of the vesicle profile). With the plots using the same scaling in the arc-length, one can see that with a larger adhesion strength w, the interfacial layer gets narrower and the separation between the red and blue phases becomes sharper and more dramatic.

IV. CONCLUSION

In this work, we develop a phase field model for the adhesion of the multicomponent vesicle membrane to a flat/

curved substrate. Some representative vesicle shapes are presented. The influence of c_2, which measures the contrast of the adhesion effect for the different phases, on the stability of membrane shapes is discussed here. It turns out that the multicomponent vesicle, whose lower part suffers stronger adhesion, is more stable in most cases. We also consider the phase transition from blue-red vesicle to red-blue vesicle, and the influence of other parameters such as the relative contribution of the adhesion and the bending energy. The effect of spontaneous curvature is also numerically observed by examining the adhesion of the vesicles on a curved substrate. We also present vesicle shapes corresponding to the Gaussian type adhesion potential to show that the protrusion of the vesicles into the substrates occurs if there is a lack of repulsive effect in the adhesion potential and it vanishes in the limit case $\epsilon \to 0$. Finally, we numerically examine the fact that adhesion can promote the phase separation for multicomponent vesicle membrane. In the case of adhesion induced phase separation we observe that the liquid-disordered phase localizes in the regions of the vesicle with high curvature. This was reported earlier for translationally symmetric membranes and substrates.

Although the numerical studies presented here are focused on the axisymmetric configuration, the phase field formulation is applicable to more general settings such as in the study of the interaction between the multicomponent vesicle and a patterned substrate. It can also be used to extend the study of membrane-mediated particle interactions [18,19] to multicomponent vesicles. The present phase field formulation of the multicomponent vesicle and substrate interaction can also be extended in several directions. For instance, by incorporating the Gaussian curvature contributions to the bending energy, fusion of multicomponent vesicles can be studied. By adding an entropic contribution to the free energy, we can also consider the weak adhesion regime where fluctuation of the vesicle shape due to thermal excitation plays an important role.

ACKNOWLEDGMENTS

Authors would like to thank anonymous reviewers for valuable comments and suggestions. The research is supported in part by NSF DMS 0712744 and by NIH NCI 1R01CA125707-01A1.

APPENDIX: ASYMPTOTIC ANALYSIS FOR η

In Sec. III, the convergent behavior of the adhered vesicles as the interfacial width ϵ approaches zero is briefly mentioned. It is claimed that the phase field function η approaches $\tanh(\frac{s-s_0}{\sqrt{2}\xi})$ as the parameter ξ approaches zero. A boundary layer calculation is carried out to support such an observation [46].

The lipid density function $\eta(s)$ is governed by the Eq. (17) and can be rewritten as

$$\xi(c_1[H-a(1+c_3\eta)]^2-2ac_3\tilde{H}+\tau-c_2wP)r + \sigma[-\xi^2(\eta' r)'+(\eta^2-1)\eta r]=0 \tag{A1}$$

An asymptotic analysis in the sharp interface limit is carried out as follows. For simplicity, we only consider the O(1) terms for outer and inner layers here. The inner layer and the outer layer are the regions around the interface and away from the interface, respectively.

Within the outer layer, η does not change much with respect to the arc-length and we expand $\eta(s)$ as

$$\eta(s) \sim \eta_0(s)+\xi\eta_1(s)+\cdots, \tag{A2}$$

We substitute Eq. (A2) into Eq. (A1) and obtain an equation for η_0 at the lowest order:

$$(\eta_0^2-1)\eta_0 r=0,$$

whose solutions are $\eta_0=0$ and ± 1.

We choose $\eta=1$ and $\eta=-1$ in the two sides of the interface to represent the blue and red phases, respectively. Here, let us assume $\eta=-1$ in the side $s<s_0$; and $\eta=1$ in the side $s>s_0$.

In the inner layer, we expect η to vary rapidly from -1 to 1 and introduce a new stretched arc-length variable

$$S=\frac{s-s_0}{\xi^\mu},$$

where μ is an yet undetermined parameter. We now express η as a function of the stretched variable S and expand η as

$$\tilde{\eta}(S) \sim \tilde{\eta}_0(S)+\xi\tilde{\eta}_1(S)+\cdots. \tag{A3}$$

Notice that

$$r(s)=r(s_0+\xi^\mu S)=r(s_0)+\xi^\mu S r'(s_0)+O(\xi^{2\mu}),$$

Upon rewriting Eq. (A1) in terms of the stretched variable S and, subsequently, using Eq. (A3) we obtain

$$-\xi^{2-2\mu}r(s_0)\frac{d^2\tilde{\eta}_0}{dS^2}-\xi^{2-\mu}r'(s_0)\frac{d}{dS}\left(S\frac{d\tilde{\eta}_0}{dS}\right)+(\tilde{\eta}_0^2-1)\tilde{\eta}_0 \times[r(s_0)+\xi^\mu S r'(s_0)]+O(\xi^\mu)=0. \tag{A4}$$

There are two possible choices for μ. If μ balances the second and third terms, namely, $2-\mu=0$. Then the leading order term is

$$-r(s_0)\frac{d^2\tilde{\eta}_0}{dS^2}=0$$

which implies $\tilde{\eta}_0=aS+b$. However, this solution does not satisfy the matching conditions

$$\tilde{\eta}_0(-\infty)=\eta_0(0)=-1, \quad \tilde{\eta}_0(+\infty)=\eta_0(\hat{s})=1.$$

Another choice is to balance the first and third terms of Eq. (A4), namely, $\mu=1$, and one gets the leading order term

$$-r(s_0)\frac{d^2\tilde{\eta}_0}{dS^2}+(\tilde{\eta}_0^2-1)\tilde{\eta}_0 r(s_0)=0.$$

If the boundary condition $\tilde{\eta}_0(-\infty)=-1$, $\tilde{\eta}_0(+\infty)=+1$ are imposed, a typical solution of the above nonlinear equation, which satisfies the matching condition, is

$$\tilde{\eta}_0(S) = \tanh\left(\frac{S}{\sqrt{2}}\right).$$

Then the composite solution of Eq. (A1), given by inner solution+outer solution−matching solution, takes on the form

$$\tilde{\eta}_0(S) + \eta_0^-(s) - \eta_0^-(0) + \eta_0^+(s) - \eta_0^+(\hat{s}),$$

and explicitly

$$\eta(s) \sim \tanh\left(\frac{s - s_0}{\sqrt{2}\xi}\right) + \ldots .$$

[1] A. L. Dunehoo, M. Anderson, S. Majumdar, N. Kobayashi, C. Berkland, and T. J. Siahaan, J. Pharm. Sci. **96**, 234 (2007).
[2] *Structure and Dynamics of Membranes, Handbook of Biological Physics*, edited by R. Lipowsky and E. Sackmann (Elsevier, Amsterdam, 1995), Vol. 1.
[3] S. Das and Q. Du, Phys. Rev. E **77**, 011907 (2008).
[4] V. D. Gordon, M. Deserno, C. M. J. Andrew, S. U. Egelhaaf, and W. C. K. Poon, EPL **84**, 48003 (2008).
[5] R. Lipowsky, M. Brinkmann, R. Dimova, C. Haluska, J. Kierfeld, and J. Shillcock, J. Phys.: Condens. Matter **17**, S2885 (2005).
[6] R. Lipowsky, Nature (London) **349**, 475 (1991).
[7] C. M. Funkhouser, F. J. Solis, and K. Thornton, Phys. Rev. E **76**, 011912 (2007).
[8] U. Seifert and R. Lipowsky, Phys. Rev. A **42**, 4768 (1990).
[9] U. Seifert, Phys. Rev. A **43**, 6803 (1991).
[10] U. Seifert and S. A. Langer, Biophys. Chem. **49**, 13 (1994).
[11] U. Seifert, Adv. Phys. **46**, 13 (1997).
[12] A.-S. Smith, E. Sackmann, and U. Seifert, EPL **64**, 281 (2003).
[13] I. Cantat, K. Kassner, and C. Misbah, Eur. Phys. J. E **10**, 175 (2003).
[14] D. Ni, H. Shi, and Y. Yin, Colloids Surf., B **46**, 162 (2005).
[15] C. Dietrich, M. Anglova, and B. Pouligny, J. Phys. II **7**, 1651 (1997).
[16] R. Lipowsky and H.-G. Döbereiner, EPL **43**, 219 (1998).
[17] M. Deserno and W. M. Gelbart, J. Phys. Chem. B **106**, 5543 (2002).
[18] M. Deserno and T. Bickel, EPL **62**, 767 (2003).
[19] M. Deserno, Phys. Rev. E **69**, 031903 (2004).
[20] J. Zhang, S. Das, and Q. Du, J. Comput. Phys. **228**, 7837 (2009).
[21] F. Julicher and R. Lipowsky, Phys. Rev. E **53**, 2670 (1996).
[22] W. Helfrich, Z. Naturforsch. **28c**, 693 (1973).
[23] T. Baumgart, S. Das, W. W. Webb, and J. T. Jenkins, Biophys. J. **89**, 1067 (2005).
[24] T. Baumgart, S. Hess, and W. W. Webb, Nature (London) **425**, 821 (2003).
[25] S. Das, Ph.D. thesis, Cornell University, 2007.
[26] Q. Du, C. Liu, and X. Wang, J. Comput. Phys. **198**, 450 (2004).
[27] Q. Du, C. Liu, R. Ryham, and X. Wang, Communications on Pure and Applied Analysis **4**, 537 (2005).
[28] T. Biben, K. Kassner, and C. Misbah, Phys. Rev. E **72**, 041921 (2005).
[29] F. Campelo and A. Hernandez-Machado, Eur. Phys. J. E **20**, 37 (2006).
[30] J. S. Sohn, Y. H. Tseng, S. Li, A. Voigt, and J. S. Lowengrub, J. Comput. Phys. **229**, 119 (2010).
[31] X. F. L. Gao and H. Yao, J. Comput. Phys. **228**, 4162 (2009).
[32] X. Wang and Q. Du, J. Math. Biol. **56**, 347 (2008).
[33] J. S. Lowengrub, A. Ratz, and A. Voigt, Phys. Rev. E **79**, 031926 (2009).
[34] S. Das and J. T. Jenkins, J. Fluid Mech. **597**, 429-448 (2008).
[35] J. T. Jenkins, J. Math. Biol. **4**, 149 (1977).
[36] R. Lipowsky and U. Seifert, Mol. Cryst. Liq. Cryst. **202**, 17 (1991).
[37] M. Kraus, U. Seifert, and R. Lipowsky, EPL **32**, 431 (1995).
[38] T. S. Ursell, W. S. Klug, and R. Philips, Proc. Natl. Acad. Sci. U.S.A. **106**, 13301 (2009).
[39] S. L. Das, J. T. Jenkins, and T. Baumgart, EPL **86**, 48003 (2009).
[40] R. Parthasarathy, C. Yu, and J. Groves, Langmuir **22**, 5095 (2006).
[41] R. Parthasarathy and J. Groves, Soft Matter **3**, 24 (2007).
[42] B. Różycki, T. R. Weikl, and R. Lipowsky, Phys. Rev. Lett. **100**, 098103 (2008).
[43] T-Y. Yoon, C. Jeong, S. Lee, J. Kim, M. Choi, S. Kim, M. Kim, and S. Lee, Nature Mater. **5**, 281 (2006).
[44] A. Roux, D. Cuvelier, P. Nassoy, J. Prost, P. Bassereau, and B. Goudh, EMBO J. **24**, 1537 (2005).
[45] J. Blowey and C. Elliott, Proceedings of the International Conference on Motion by Mean Curvature and related Topics, Trento, July 20–24, 1992, (Walter de Gruyter, Berlin, 1994), Vol. 1.
[46] M. H. Holmes, *Introduction to Perturbation Methods, Texts in Applied Mathematics 20* (Springer-Verlag, Berlin, 1995).